2. Investigations for Low Prandtl Fluid

2.1 Numerical Simulation of Three Dimensional Oscillatory Flow in Half-Zone Bridges of Low Pr Fluids

Nobuyuki Imaishi
Kyushu University

NUMERICAL SIMULATION OF THREE DIMENSIONAL OSCILLATORY FLOW IN HALF-ZONE BRIDGES OF LOW Pr FLUIDS

Nobuyuki Imaishi*, Shouich Yasuhiro* and Shinichi Yoda**

*Institute of Advanced Material Study, Kyushu University, Kasuga, 815-8580
**NASDA, Sengen 2-1-1, Tsukuba 305-8505

ABSTRACT In order to understand the realistic flow transitions in a small liquid bridge of molten tin with an aspect ratio of As=2.0, which was used for experiments at NASDA, a long-run numerical simulation was conducted using real temperature history of the experiment for boundary conditions in our numerical code. The result revealed that the critical Marangoni numbers, flow mode and frequency of the 3-D flow of the present ramped ΔT case are very close to those obtained in our previous works in which ΔT was kept constant. However, the amplitude of surface temperature oscillations near the second critical point are very small (0.2K) and its frequency is high (2.5Hz in 1-T type oscillation). At highly super critical state, the "1-T" type oscillatory flow-temperature structures started slow azimuthal motion. This rotation caused a low frequency oscillation of a local surface temperature. At further large ΔT, there occurred an alternative changes of oscillation mode between 1-T and 2-T, whereas the slow rotation action was maintained. These results seem to explain the experimental observations.

We also conducted a set of Proper Orthogonal Decomposition (POD) analyses for oscillatory flows in liquid bridges of low Pr fluid. POD helped understanding the detailed structures of the 3-D disturbances in a liquid bridge of Pr=0.01 fluid simulated with a condition of As=2.0 and Ma=35.0.

Keywords: Marangoni flow, Numerical simulation, Three dimensional oscillatory flow, Critical Marangoni number, Molten tin, Flow mode, Proper Orthogonal Decomposition

1. INTRODUCTION

Since 1999, we have conducted a series of numerical simulations of unsteady three dimensional Marangoni convection in a half-zone liquid bridge of low Prandtl number (Pr) fluids [1-11]. In the first few years, we used a very simple model of liquid bridge in which a liquid bridge is confined between two differentially heated solid discs of infinitely large thermal conductivity, i.e., the disc temperature is uniform over each disc surface area, and the disc temperatures are kept constant at each temperature at t>0. With this simple model of liquid bridge, we determined the first and the second critical Marangoni numbers as a function of the aspect ratio, $As=L/a$; where L is the length and a is the radius of the liquid bridge. Characteristics of the oscillatory flow in liquid bridge of low Pr fluid is its two-step flow transition process, i.e., the first instability breaks the spatial axisymmetry (but the flow regime is still steady) prior to the onset of time dependent flow field. Rupp et al.[12], Levenstan [13, 15], Leypoldt et al. [14] reported their numerical simulations of oscillatory Marangoni flow in low Pr fluid and confirmed the two-steo instability process for a limited range of the aspect ratios mostly As=1.0 and 1.2.

We have conducted series of numerical simulations of Marangoni convection in half-zone liquid bridges of low Prandtl number fluids for a wide range of aspect ratio (As=0.6 – 2.2)[5,7]. Our numerical code was validated by comparing the critical Marangoni (or Reynolds number) to the linear stability analysis and other numerical results. Drawings of the flow and temperature fields and oscillations of local velocities and temperatures reported in

previous Annual Reports [6, 8] helped understanding the behaiviors of oscillations of velocity and temperature fields, different oscillation types, modes of the oscillatory Marangoni flow in low *Pr* liquid bridges. We determined the first and the second critical Reynolds numbers as a function of aspect ratio and the Prandtl number. Our results indicate that the critical temperature difference (ΔTc) for the incipience of oscillatory flow in liquid bridge of low Prandtl fluid increases as the aspect ratio decreases and shows maximum value at As=1.2. This trend has not confirmed experimentally. There have been very few reports of experimental observation of oscillatory Marangoni flow in low pr liquid bridge; mercury [17], semiconductor melt[16, 18- 27, 29, 30] and molten tin [28, 32]. These authors reported oscillations of local surface temperature under certain large ΔT, vibrations of liquid surface, and non-axisymmetric trajectories of tracer particles. The research group at NASDA reported slow and fiast oscillations of local surface temperature [32-34]. They defined the critical condition for incipienc of oscillatory flow by the ΔT at which they detected these temperature oscillations, either slow or fast. They measured ΔT by using two thermocouples molded in the suport rods and the junctions are located δ=0.5mm apart from the melt/rod interface. Although the distance is as small as 0.5mm, temperature drops in the distance δ is significantly large since very large heat flux flows through the rod and liquid bridge. In the FY2001 Annual Report [8], we reported a conduction dominant model which estimated the conduction temperature drop in the small distance δ and enabled to properly evaluate the effective temperature differnce acting on the liquid surface. The conduction temperature drop causes a serious error in the critical Marangoni number, some time as large as 200%. Despite these corrections, there remained some discrepancies between our simulation results and the experiments. First one is the frequencies of local temperature oscillations. Numerical results predicted the critical frequency of $\approx$1.9Hz for a small tin bridge with a=1.5mm and As=2.0. On the other hand, experimentally observed frequency was 0.2Hz or 0.02Hz. In many experimental runs, very slow oscillations ($\approx$0.02Hz) of local temperature were first detected and last for a while and then took over by another type of oscillations with medium frequenciess ($\approx$0.2Hz). Our simultions conducted in FY2001 could not explain these oscillations with slow and the medium frequencies. Previous simulations had been conducted over a limited range of ΔT (near the second critical ΔT) and run-time (corresponded to less than few minutes of real experimental run). The second one is the value of the second critical Marangoni number. The experimentally determoned second critical Marangoni number, based on the effective temperature difference corrected by the conduction dominant model, tend to be larger than those predicted by our simulation [8].

In FY 2002, we tried a simulation for a liquid bridge of As=2.0 under a experimental history of temperature difference over 10 minutes of experimental run time, in order to reveal what phenomena correspond to these slow oscillations and when the oscillatory flow started.

In FY2003, we also conducted a Properly Ortthogonal Decomposition (POD) of the oscillatory flow in order to reveal the tempo-spatial structures of the oscillating velocity and temperature fields. In order to understand the behavior of complicated flows, we use direct numerical simulation (DNS) of the partial differential equations. Three-dimensional (3-D) DNS usually consumes much time and computation fees. Often the results of DNS involve so many types of disturbances. The flow and temperature fields obtained by DNS in our previous reports will be analyzed (decomposed) by means of the POD method to get better understandings of characteristic modes and their spatial structures of the three dimensional disturbances.

2. NUMERICAL SIMULATION USING EXPERIMENTAL TEMPERATURE HISTORY

2.1 MODEL FORMULATIONS

In order to evaluate the effect of thermal resistance in the supporting solid rods extending both sides of the liquid bridge, cylindrical solid rods are added to a standard model of half-zone liquid bridge, as shown in **Fig. 1**. The origin of the z axis is located at the center of the lower melt/rod interface. The length of the liquid bridge is $a\times As$, the length of the rods are $a\times As_r$. The liquid surface is assumed non-deformable and cylindrical. This shape is true under microgravity condition. There acts the Marangoni effect on the liquid surface. Radiative heat loss from surfaces was neglected in the present simulation. Fundamental equations, initial and boundary conditions are expressed as follows.
In the liquid bridge:

$$\frac{U}{R}+\frac{\partial U}{\partial R}+\frac{1}{R}\frac{\partial V}{\partial \theta}+\frac{\partial W}{\partial Z}=0 \tag{1}$$

$$\frac{\partial U}{\partial \tau}+U\frac{\partial U}{\partial R}+\frac{V}{R}\frac{\partial U}{\partial \theta}-\frac{V^2}{R}+W\frac{\partial U}{\partial Z}=-\frac{\partial P}{\partial R}+\frac{\partial}{\partial R}\left\{\frac{1}{R}\frac{\partial (RU)}{\partial R}\right\}+\frac{1}{R^2}\frac{\partial^2 U}{\partial \theta^2}-\frac{2}{R^2}\frac{\partial U}{\partial \theta}+\frac{\partial^2 U}{\partial Z^2} \tag{2}$$

$$\frac{\partial V}{\partial \tau}+U\frac{\partial V}{\partial R}+\frac{V}{R}\frac{\partial V}{\partial \theta}+\frac{UV}{R}+W\frac{\partial V}{\partial Z}=-\frac{1}{R}\frac{\partial P}{\partial \theta}+\frac{\partial}{\partial R}\left\{\frac{1}{R}\frac{\partial (RV)}{\partial R}\right\}+\frac{1}{R^2}\frac{\partial^2 V}{\partial \theta^2}+\frac{2}{R^2}\frac{\partial V}{\partial \theta}+\frac{\partial^2 V}{\partial Z^2} \tag{3}$$

$$\frac{\partial W}{\partial \tau}+U\frac{\partial W}{\partial R}+\frac{V}{R}\frac{\partial W}{\partial \theta}+W\frac{\partial W}{\partial Z}=-\frac{\partial P}{\partial Z}+\frac{1}{R}\frac{\partial}{\partial R}\left(R\frac{\partial W}{\partial R}\right)+\frac{1}{R^2}\frac{\partial^2 W}{\partial \theta^2}+\frac{\partial^2 W}{\partial Z^2} \tag{4}$$

$$\mathrm{Pr}\left(\frac{\partial \Theta}{\partial \tau}+U\frac{\partial \Theta}{\partial R}+\frac{V}{R}\frac{\partial \Theta}{\partial \theta}+W\frac{\partial \Theta}{\partial Z}\right)=\frac{1}{R}\frac{\partial}{\partial R}\left(R\frac{\partial \Theta}{\partial R}\right)+\frac{1}{R^2}\frac{\partial^2 \Theta}{\partial \theta^2}+\frac{\partial^2 \Theta}{\partial Z^2} \tag{5}$$

In the solid rods,

$$\mathrm{Pr}\frac{\partial \Theta}{\partial \tau}=\alpha_{m/r}\left\{\frac{1}{R}\frac{\partial}{\partial R}\left(R\frac{\partial \Theta}{\partial R}\right)+\frac{1}{R^2}\frac{\partial^2 \Theta}{\partial \theta^2}+\frac{\partial^2 \Theta}{\partial Z^2}\right\} \tag{6}$$

Initial conditions:

$$U=V=W=0,\quad \Theta=1 \tag{7, 8}$$

Boundary conditions:
At the upper end of the upper rod ($Z=As+As_r$):

$$\Theta=\Theta_{H(\tau)} \tag{9}$$

At the bottom of the lower rod ($Z=-As_r$)

$$\Theta=\Theta_{C(\tau)} \tag{10}$$

At the surface of the liquid bridge ($R=1$):

$$U=0,\quad \frac{\partial W}{\partial R}=\mathrm{Re}_T\frac{\partial \Theta}{\partial Z},\quad \frac{\partial}{\partial R}\left(\frac{V}{R}\right)=\mathrm{Re}_T\frac{1}{R}\frac{\partial \Theta}{\partial \theta},\quad \frac{\partial \Theta}{\partial R}=0 \tag{11,12,13,14}$$

At the surface of the rods (R=1):

$$\frac{\partial \Theta}{\partial R} = 0 \tag{15}$$

At the upper melt/rod interface (Z=As)

$$U = V = W = 0, \quad \frac{\partial \Theta}{\partial Z} = \lambda_{r/m} \frac{\partial \Theta}{\partial Z}\Big|_{in\ rod} \tag{16, 17}$$

At the lower melt/rod interface (Z=0)

$$U = V = W = 0, \quad \frac{\partial \Theta}{\partial Z} = \lambda_{r/m} \frac{\partial \Theta}{\partial Z}\Big|_{in\ rod} \tag{18,19}$$

The non-dimensional parameters are the Prandtl number, Reynolds number, respectively defined as follows.

$$Pr = \frac{\nu}{\alpha} = \frac{C_p \cdot \mu}{\lambda},$$

$$Re_T = -\left(\frac{\partial \sigma}{\partial T}\right) a T_{C0} \Big/ (\mu \nu).$$

The Marangoni number is defined as Ma_T=$Re_T Pr$. The non-dimensional variables are defined as; $\{R, Z\} = \{r/a, z/a\}$, $P = pa^2/(\nu\mu)$, $U = ua/\nu$, $\tau = t\nu/a^2$, $\Theta = T/T_{C0}$ where, $\alpha = \lambda/c_p\ \rho$. , u: velocity, p: pressure, c_p: heat capacity, ρ: density, λ: thermal conductivity, μ: viscosity, ν: kinematic viscosity, T_{C0} the initial temperature of the cold end of the supporting rod, σ: the Stefan-Boltzman constant and $\alpha_{r/m} = \alpha_r / \alpha_m$, $\lambda_{r/m} = \lambda_r / \lambda_m$.

2.2 NUMERICAL METHOD

These equations are discretized by a finite difference method with a modified central difference treatment for the convective terms [35] and non-uniform staggered grids. Non-uniform grids were adopted to increase the resolution. The radial velocities on the central axis were calculated by means of the method of Ozoe et al. [36]. A fully implicit code was developed last year using the Conjugate Gradient method, combined with a specially coded matrix pre-conditioner, as reported in 2001 Annual Report [8]. This code provides very fast calculation, however, works only on the super computer. The thermophysical properties and geometric parameters are listed in **Table 1**. The simulation results will be expressed in dimensional form for the sake of easy comparison with the experimental results. In this work, we used the same grid as was used last year for As=2.0 [8,11].

The temperatures on both ends of the model must be given as a function of time. In this work, we reduced this information from one of the time records of NASDA's experiments measured by two thermocouples mounted in the supporting rods on the axis but δ apart from the melt/rod interfaces. The temperatures at both ends of the rods with a length As_r=L_r/a=2 were deduced using a conduction dominant model.

Based on the records of thermocouple data [37], $T'_c(t)$ and $T'_h(t)$, conduction dominant model gives reasonable estimates of $T_C(t)$ and $T_H(t)$, as follows.

$$T_C(t) = T_c'(t) - \left(\frac{L_r - \delta}{\lambda_r}\right)\left(\frac{T_h'(t) - T_c(t)'}{\frac{L}{\lambda_m} + \frac{2\delta}{\lambda_r}}\right) \tag{20}$$

$$T_H(t) = T_h'(t) + \left(\frac{L_r - \delta}{\lambda_r}\right)\left(\frac{T_h'(t) - T_c(t)'}{\frac{L}{\lambda_m} + \frac{2\delta}{\lambda_r}}\right) \tag{21}$$

In the present simulation, we used the following geometric parameters: a=1.5mm, L=L_r=3.0mm and d=0.5mm. Thus obtained and smoothed results of T_H and T_C are shown in Fig. 2 as a function of time. T_H and Tc rise in the first period, however, the temperature difference is monotonically increasing throughout the run.

2.3. RESULTS

Results of the simulation sing the temperature records of the top and bottom temperatures during the experiment are shown in Figs. 3-7.

Fig. 3 shows time evolutions of local values of the axial velocity, azimuthal velocity on the melt surface, averaged azimuthal velocity, local temperatures, together with the imposed over-all temperature difference ΔT_T, calculated temperature difference between the two thermocouple positions ΔT" and the effective temperature difference acting on the melt surface, ΔT_e which is defined as.

$$\Delta T_e = \left\{\int_0^{2\pi} \Theta_{(1,\theta,0)} d\theta - \int_0^{2\pi} \Theta_{(1,\theta,As)} d\theta\right\} T_{C0} / 2\pi \tag{22}$$

An averaged azimuthal velocity on the surface was defined as

$$|\bar{U}_\vartheta| = \left|\int_0^{2\pi} U_{\vartheta(1,\theta,0.5)} d\theta\right| / 2\pi \tag{23}$$

$|\overline{U}_\vartheta|$ was chosen as an indicator of the flow oscillations in 1-T type. If the flow field is steady in m=1 mode, $|\overline{U}_\vartheta|$ must be zero. But flow field becomes oscillatory in 1-T mode, $|\overline{U}_\vartheta|$ is expected to oscillate around zero.

Fig. 3 suggests that there occurred two-step flow transitions in the liquid bridge. The first one is a transition from an axisymmetric flow to a three dimensional flow. The second one is an incipience of oscillatory flow.

Fig.4 shows results for very early period. In this simulation, as an initial condition, we imposed a finite temperature difference ΔT_T=3.4K. Then, there was an initial transient period continued for 3 seconds to develop conductive and convective temperature and flow fields of Marangoni flow in the melt zone. The temperature and velocity fields were all axisymmetric. As the over-all temperature difference increased, the flow velocity increased gradually. At about t=15 seconds, a local azimuthal velocity started increasing with time indicating a growth of a 3-D disturbance. Growth process continued. At around t=56sec., 3-D disturbance became somehow observable and at around t=66sec, it reached fully developed stage. Since ΔT_T was increasing, the strength of the flow field was gradually increasing thereafter, but the flow mode was maintained. Detailed analysis of velocity and temperature fields revealed that the fundamental azimuthal wave number of this 3-D flow and temperature field was m=1. This 3-D non-oscillatory Marangoni flow was maintained stable. Since this flow field is almost symmetrical with respect to one diameter, an averaged azimuthal velocity ($|\overline{U}_\vartheta|$) showed very small value, about 5×10^{-8}, at t=60sec and decreased slowly.

Now, we should make some discussions on the critical conditions for the flow transitions based on the present simulation. It is difficult to define the critical point accurately in Fig.4. However, the axisymmetric flow field become unstable against a 3-D disturbance at

sometime between t=15sec. and 30sec. The effective temperature difference then was ΔT_e= 0.87K at 15sec. and 1.05K at 30sec., respectively. Then, the first critical Marangoni number, based on the effective temperature difference (ΔT_e), ranges between 5.96 and 7.21. These are very close to our previous result; Ma_{c1}= 7.13 [11].

On the other hand, in the 2001 Annual Report, we reported the second critical Marangoni number Ma_{c2}=25.36 and critical frequency ω_c=136.4 (i.e., f=1.87Hz for a molten tin bridge of a=1.5mm) for a molten tin bridge of As=2.0 based on the simulations assuming time-independent over all temperature difference without rods [11].

Fig. 3 shows that at t=160sec. (ΔT_e =3.94K, Ma=27.04) the averaged azimuthal velocity ($|\overline{U}_\vartheta|$) increased again up to 2×10^{-8} but no oscillation was observed. However, at t=190sec. (ΔT_e=4.45K, Ma=30.54), $|\overline{U}_\vartheta|$ started oscillation with a frequency f=1.9Hz and its amplitude and frequency increased with time very quickly and oscillation amplitude of $|\overline{U}_\vartheta|$ became almost constant at t=220sec. Frequency of local temperatures and U_θ was gradually increased with time (i.e., increase of ΔT_e) from 1.9Hz to 2.53Hz at t=250sec. Detailed visualizations revealed that the oscillations between t=190 and 220sec. is characterized as 1-T type; fundamental wave number is m=1 and the line of symmetry shows periodical twisting back and forth in azimuthal direction. However, it is difficult to distinguish the oscillatory behavior from the plot of local surface temperatures in Fig.3, even on an enlarged plot in Fig.5, since the amplitude of temperature oscillations was less than 0.1K in this stage.

However, at t=250sec., local temperature oscillations were modulated by slow oscillations with large amplitudes ($\approx$1K). Enlarged plots in Fig.5 and the FFT spectraum clearly show that the low frequency oscillations ($f\approx$0.04Hz) and high frequency oscillations ($f\approx$2.5Hz) are coexisting. Visualizations of the flow and temperature fields in the liquid bridge revealed that the high frequency oscillation corresponds to the 1-T type oscillations. The low frequency oscillation corresponds to a rotation of the whole body of the 3-D oscillating fields in azimuthal direction. This type of oscillatory Marangoni flow in half-zone liquid bridge was first recognized in this work. We named this oscillation as "1-T+R" type where R stands for "rotation".

As shown in Fig.6, after several oscillations of low frequency, at t=365sec., the surface temperature started rather random oscillations with large amplitude ($\approx$1K of peak-to-peak value) and medium frequency ($f\approx$0.25Hz) with small amplitudes (less than 0.2K). Visualizations of the flow and temperature distributions in the liquid bridge revealed that these oscillations were caused by temporal changes of flow modes between 1-T and 2-T accompanied by an irregular rotating motion. This type of oscillations of surface temperature may correspond to the experimentally observed temperature oscillations with $f\approx$0.29Hz under a range of the Marangoni number between Ma=73 and 90.

Alternations of the flow modes continued for 35 sec. in this simulation. At t=400sec., the oscillation mode changed again. At t>400sec., oscillations in 1-T mode was dominant, but sometime, mode changes to 2-T type for a short period and soon come back to 1-T type. Angle of the line of symmetry changed quickly in azimuthal direction accompanying the mode change. However, the grids used in the present simulation are rather too coarse to guarantee the accuracy of simulation results at this highly super critical conditions.

The present simulation results first succeeded to explain the NASDA's experimental results quantitatively. As reported in the 2001 Annual Report [8], NASDA's experiments for a molten tin bridge of As=2.0 experienced very strange slow oscillations of local temperature on the liquid bridge (order of the frequency: 0.01Hz) prior to the incipience of a series of higher oscillations (order of the frequency: 0.2Hz). On the other hand, our previous simulations predicted Ma_{c2}=25.36 and critical frequency ω_c=136.4 (i.e., f=1.87Hz for a

molten tin bridge of a=1.5mm) for a molten tin bridge of As=2.0 based on the simulations assuming time-independent over all temperature difference without rods. In FY20021, we thought the observed oscillations of $f \approx 0.2$Hz might correspond to the oscillations predicted by the simulation and simulation results could not explain low frequency oscillations.

The present simulation revealed that the incipience of oscillatory flow might have started prior to the slow frequency oscillations but it had not been detected. In order to detect the second critical condition (incipience of the oscillatory flow) a very sensitive temperature sensors are required, because the surface temperature oscillates with rather high frequency ($\approx$2.5Hz) and small amplitudes (less than 0.1K PP). Present result draw realistic explanations of the flow phenomena that caused the oscillations of surface temperatures with low frequency ($\approx$0.01Hz) and another oscillation with medium frequency range ($\approx$0.25Hz).

However, present simulation could not resolve the issue of the second critical Marangoni number. As mentioned before,
the second critical Marangoni number would be Ma_{c2}=31.2, if we define the critical point as the time when $|\overline{U}_\vartheta|$ starts its oscillations, i.e., t=190sec. in the present case. This result is slightly larger than the previous result, i.e., Ma_{c2}=25.36 [11].

In the transient simulations, one may think that the critical condition depend on the rate of the temperature ramp and also geometry of the liquid bridge. Here, we checked the effect of the rate of temperature ramp on the incipience of the oscillatory flow. Fig. 7 shows growth process of $|\overline{U}_\vartheta|$ under four different ramp rates. In these simulations, the initial condition was the instantaneous distributions of velocity, pressure and temperature at t=180sec. (ΔT_e=4.2K, Ma=28.8) shown in Fig. 2. We used following four rates of temperature ramp; case 1) nominal value shown in Fig. 2 ($d\Delta T_T/dt$=0.025K/s.), case 2) $d\Delta T_T/dt$=0, 3) $d\Delta T_T/dt$=0.05K/s., and case 4) $d\Delta T_T/dt$= 0.075K/s. As the ramp rate increases, growth rate of the amplitude of $|\overline{U}_\vartheta|$ increases and may more quickly attain to a observable amplitude. It should be noted that even if we maintain the ΔT_T constant at Ma=28.8 (Case 1), the non-oscillating 3-D flow was unstable at and oscillatory disturbance started after long waiting time. This indicates that the ΔT_T=4.2K at t=180 sec. (Ma=28.8) was already in a super critical condition according to our definition of the critical condition, i.e., the marginal stability condition.

Results shown in Fig.7 indicate that regardless the rate of temperature ramp, oscillatory disturbance starts its growth process at around t=190sec. in the present simulations. These results suggest that we can not define an unique value of Ma_{c2} from the time when the oscillatory disturbance started i.e., Ma_{c2}=30.40, 32.25 and 33.63, for Case 1). Case 3) and Case 4), respectively. These suggest that in order to initiate oscillations, an embryo of oscillatory disturbance must be incubated, otherwise the 3-D non-oscillating flow can be maintained at a super critical state. In the previous simulations, we adopted an isothermal, quiescent initial condition. Such an initial condition created considerably large initial disturbance which may work as an embryo and the oscillations could started quite soon with very small super critical ΔT. Of course, such disturbances could not grow under sub-critical conditions. On the other hand, the present simulation used monotonically and slowly increasing ramped temperature difference the 3-D non-oscillating flow was developed with less disturbances and lacked in such embryo which may initiate an oscillatory flow. Thus, the 3-D non-oscillating flow field was maintained until t=190 sec. in a super critical state.

On the other hand, if we assume that the oscillation becomes observable at a moment when $|\overline{U}_\vartheta|$ reaches 1×10^{-4}, Fig. 7 suggests that the critical Marangoni numbers may become strongly dependent on the temperature ramp rate, i.e., Ma_{c2}=34.08, 36.85 and 39.87, for Case 1, Case 3 and Case 4, respectively. These values are considerably larger than our previous

result, Ma_{c2}=25.36 decided as a marginal stability condition based on a series of simulations under constant ΔT's [11].

3. POD ANALYSIS OF 3-D DISTURBANCES

3. 1 FUNDAMENTALS OF THE POD

POD is well known as a rigorous procedure for extracting a basis of characteristic modes from sampled time evolution signals [38-44]. These modes are the eigenfunctions of an integral operator based on the spatial correlation function. They are shown to form an orthogonal basis for the function space in which the process resides, and to represent this process in the most efficient way [41,42]. Directly applying this procedure to a 3D discretized problem involves extremely considerable computing task because the spatial correlation matrix (the eigenvalues of which we want to obtain) is usually very large. For the case under consideration in our study, the matrix would have a dimension corresponding to the number of grid points used for the DNS scalculation. A more accessible approach which is referred to as the method of snapshots was proposed by Sirovich [40]. This method which invokes the ergodic hypothesis allows to reduce the computation task to a much more tractable eigenproblem with a size N equal to the number of snapshots of the flow field which have been obtained by direct numerical simulation (usually of the order of some hundreds). The method of snapshots [45] which is applied to our problem is presented in a practical way in the following.

The state variables $U(\mathbf{x},\tau)$ and $\Theta(\mathbf{x},\tau)$ obtained through the N snapshots are decomposed into time-averaged parts, $\overline{U}(\mathbf{x})$ and $\overline{\Theta}(\mathbf{x})$, and time-varying parts, $U'(\mathbf{x},\tau)$ and $\Theta'(\mathbf{x},\tau)$, i.e.,

$$U(\mathbf{x},\tau)=\overline{U}(\mathbf{x})+U'(\mathbf{x},\tau), \tag{24}$$

$$\Theta(\mathbf{x},\tau)=\overline{\Theta}(\mathbf{x})+\Theta'(\mathbf{x},\tau). \tag{25}$$

The two time correlation matrices $C^{U}_{m,n}$ and $C^{\Theta}_{m,n}$ are then constructed from the velocity and temperature samples, respectively, as

$$C^{U}_{m,n}=\frac{1}{N}(U'(\mathbf{x},\tau_m),U'(\mathbf{x},\tau_n)) \quad m,n=1,2,...,N \tag{26}$$

$$C^{\Theta}_{m,n}=\frac{1}{N}(\Theta'(\mathbf{x},\tau_m),\Theta'(\mathbf{x},\tau_n)) \quad m,n=1,2,...,N \tag{27}$$

where the outer parentheses $(\,.,.\,)$ represent the inner product defined as

$$(a,b)=\int_D a(x)\cdot b(x)dx \tag{28}$$

where a and b are two vectors for Eq. (27) and two scalars for Eq. (28) and D is the flow domain.

The eigenvalues λ^{U}_i and λ^{Θ}_i associated to these matrices, and their corresponding eigenvectors A^m_i and B^m_i, $m=1,N$, can be calculated, which gives

$$C^{\mathrm{U}}_{m,n}A^n_i=\lambda^{\mathrm{U}}_i A^m_i \tag{29}$$

and

$$C^{\Theta}_{m,n}B^n_i=\lambda^{\Theta}_i B^m_i. \tag{30}$$

Finally, the characteristic modes (also called empirical eigenfunctions) $\Phi^{\mathrm{U}}_i(\mathbf{x})$ and $\Phi^{\Theta}_i(\mathbf{x})$ (here normalized) are obtained as linear combinations of the time-varying parts,

$$\Phi^{\mathrm{U}}_i(\mathbf{x})=\sum_{m=1}^{N}A'^m_i\mathrm{U}'(\mathbf{x},\tau_m) \tag{31}$$

and $$\Phi_i^{\Theta}(\mathbf{x}) = \sum_{m=1}^{N} B_i'^m \Theta'(\mathbf{x}, \tau_m), \tag{32}$$

with $A_i'^m = A_i^m / \sqrt{\lambda_i^{\mathrm{U}} N \sum_{m=1}^{N} (A_i^m)^2}$ and $B_i'^m = B_i^m / \sqrt{\lambda_i^{\Theta} N \sum_{m=1}^{N} (B_i^m)^2}$.

The method chosen here is based on the separate treatment of velocity and temperature with the construction of a two time correlation matrix for each field, as is also done in Refs. 42-44.

The eigenvalues and empirical eigenfunctions have interesting properties:

1) The eigenvalues are real, non-negative and can be ordered. Each eigenvalue λ_i^{U} (or λ_i^{Θ}) represents the relative contribution of the corresponding modes $\Phi_i^{\mathrm{U}}(\mathbf{x})$ (or $\Phi_i^{\Theta}(\mathbf{x})$) to the total fluctuation kinetic energy (or thermal energy).

2) The eigenfunctions are orthogonal and have been normalized, so that they verify $(\Phi_i^{\mathrm{U}}, \Phi_j^{\mathrm{U}}) = \delta_{i,j}$ and $(\Phi_i^{\Theta}, \Phi_j^{\Theta}) = \delta_{i,j}$.

3) The velocity eigenfunctions are divergence-free ($\nabla . \Phi_i^{\mathrm{U}} = 0$) since they are constructed as linear combinations of the incompressible flow snapshots v'.

4) At last, from Eqs. (24) and (31), and Eqs. (25) and (32), it is easy to understand that the eigenfunctions automatically satisfy the homogeneous boundary conditions associated to the perturbations for the problem under consideration.

The time-varying parts $v'(x,\tau)$ and $T'(x,\tau)$ can then be expressed in terms of these normalized eigenfunctions as

$$U'(\mathbf{x},\tau) = \sum_{i=1}^{M_V} a_i(\tau) \Phi_i^{\mathrm{U}}(\mathbf{x}) \tag{33}$$

$$\Theta'(\mathbf{x},\tau) = \sum_{i=1}^{M_T} b_i(\tau) \Phi_i^{\Theta}(\mathbf{x}) \tag{34}$$

where $a_i(\tau)$ and $b_i(\tau)$ are coefficients depending on time, and M_V and M_T are the numbers of the first most important modes retained in the expansion for velocity and temperature, respectively. When $M_V = M_T = N$, the original sampled signal can be reproduced exactly, with

$$a_i(\tau) = a_i^m = N \lambda_i^U A_i'^m \quad \text{and} \quad b_i(\tau) = b_i^m = N \lambda_i^{\Theta} B_i'^m. \tag{35}$$

Usually M_V and M_T are much smaller than the number of snapshots, N. They are chosen so that the set of eigenfunctions captures most of the fluctuation energy. For example in Sirovich[3], the choice is made by taking $\xi > 99\%$, where $\xi \equiv \sum_{i=1}^{M_U} \lambda_i^{\mathrm{U}} / \sum_{i=1}^{N} \lambda_i^{\mathrm{U}}$ or $\sum_{i=1}^{M_\Theta} \lambda_i^{\Theta} / \sum_{i=1}^{N} \lambda_i^{\Theta}$, meaning that the first M_U (M_Θ) modes capture more than 99% of the fluctuation kinetic energy (thermal energy). The use of these modes to construct a low dimensional model is presented in the next section.

Here we used a newly developed numerical code of POD and decomposed one of the DNS results obtained in FY2001[7, 8]. Calculation proceeded along the flow chart shown in Fig.8. The grid used for POD was the same as that used for DNS in our previous report. In this work, we picked up 100 to 400 data sets of velocities and temperature covering two to

four periods of oscillations of constant amplitudes.

As will be pointed out later, in most of the cases, energy of the three dimensional disturbances are contained in the first two modes. Then hereafter, we will approximate the DNS results with only two to four modes.

3.2 RESULTS OF POD ANALYSIS

Fig. 9 shows snapshots of one of our DNS results for a low *Pr* liquid bridge (*As*=2.0, *Pr*=0.01 and *Ma*=35.0). Firstly, data sets are averaged over the sampled oscillation periods to obtain time averaged fields of velocity and temperature, $\overline{U}$ and $\overline{\Theta}$, respectively. Then the time-varying parts are obtained.

The POD process was applied to decompose these time-varying parts to many modes. Fig. 10 shows snapshots of four major eigen functions of velocity, Φ^U on a horizontal cut at the middle of the liquid bridge. Here, radial and azimuthal components are indicated by the arrows and the axial velocity W is shown by the color. Amplitudes for these modes are also shown in the figure. It is understood that the first and the second modes are very much significant. Fig.11 shows bird's eye view of distributions of contour surfaces of Φ^W (the eigen functions for time-varying part of the W: z component of velocity vector).

Figs.12 and 13 show the structures of the major eigenfunctions of time-varying part of temperature disturbance together with their amplitudes.

Figs.11 and 13 reveal that Φ^W and Φ^Θ have very complex spatial structures. However, judging from the order of magnitude of the eigen vectors, the major two modes are taking important roles in this case. The sums of the major two eigenfunctions with their coefficients provide fairly good reproduction of the time-varying part of velocity and temperature disturbances, as shown in Figs.14 and 15. Snapshots of as birds eye views of the spatial distributions of contour surfaces of $\Sigma a_i\Phi_i^W$ and $\Sigma b_i\Phi_i^\Theta$ (sum of the major two terms) are shown in Fig.16. Video records of $\Sigma a_i\Phi_i^W$ and $\Sigma b_i\Phi_i^\Theta$ indicate that the disturbances periodically move in the azimuthal direction, starting from the front side of the figure and move toward the back side in each side, i.e., right and left side, respectively.

In FY2003, more precise POD will be conducted to many DNS results in order to understand the details of the origin and characteristics of the three dimensional oscillatory Marangoni flow in half-zone liquid bridges.

4. CONCLUSIONS

1) A long-run simulation was conducted to obtain a better understandings of the temperature oscillations on a molten tin liquid bridge surface observed in NASDA's ground-base experiment. The simulation used a time records of temperatures measured by two thermocouples mounted in the supporting rods made of iron, located on the axis of the rods and apart from the melt/rod interfaces by a small distance δ=0.5mm. In the present simulation, a molten tin liquid bridge with an aspect ratio *As*=2.0 was modeled being suspended between two iron rods of As=2.0 and the surfaces are adiabatic. We adopted a simple conduction dominant model to reduce the temperatures at top and bottom ends of model system from the temperature records measured by the thermocouples.

Transient simulation results revealed that the Marangoni flow in the liquid bridge experienced axisymmetric flow, non-oscillating 3-D flow with a fundamental wave number *m*=1, and 3-D oscillatory flows. The first flow mode change from an axisymmetric to a 3-D non-oscillating flow started at around t= sec. and fully grown up at around t= sec. The first critical Marangoni number Ma_{c1} lies between 5.96 and 7.21. These are very close to our previous result; Ma_{c1}= 7.13.

Oscillatory flow of 1-T type mode started its growth at around t=190 sec. from a very small amplitude and a frequency of *f*=1.9Hz. Oscillation amplitudes increased rapidly and

fully grown up at around t=220sec. At t=220sec., amplitude was about 0.1K and continuously increased its amplitude as temperature difference increase with time. However, the amplitude of surface temperature oscillation was less than 0.2K and $f \approx 2.5$Hz at t=250sec. The second critical Marangoni number was Ma_{c2}.=30.52, if we define the critical point as the instance when flow field started oscillation with very small amplitude. This value is significantly larger than our previous result, Ma_{c2}.=25.32, with a critical frequency of f_c=1.87Hz, which was determined as a marginal stability condition based on a series of simulations with time-independent values of ΔT.

Despite this discrepancy in the critical Marangoni number, the present simulation found out new type of oscillation phenomena. At t=265 sec., the whole body of the velocity and temperature fields exhibiting the 1-T type oscillations started slow rotating motion around the axis. Correspondingly, local temperatures indicated low frequency oscillations ($f \approx 0.04$Hz , amplitude $\approx$ 1K) accompanied by the high frequency oscillations of 1-T oscillations ($f \approx 2.5$Hz, amplitude $\approx$ 0.2K). These low frequency oscillations may explain the experimentally observed oscillations.

After several low frequency oscillations, the surface temperature started another type of oscillations during t=365-400 with medium frequency and large amplitudes ($f \approx 0.25$Hz, amplitudes $\approx$ 1K). These oscillations correspond to alternative changes of oscillating modes between 1-T and 2-T types. These oscillations may explain the second temperature oscillations observed in the experiment after the low frequency oscillations faded out.

The present simulation predicted third type of oscillations at t>400sec. In this stage, 1-T type oscillations are dominant but for a short time, 2-T type oscillations took over accompanied by a big jumps of local surface temperatures. This type of temperature oscillations was not reported in the experiments to date. The grids used in this simulation were not fine enough for calculations at highly super critical condition and the results are not completely reliable. Further check and validations are necessary.

2) A Proper Orthogonal Decomposition (POD) method was applied to one of our previous results of the direct numerical simulation (DNS) of the oscillating Marangoni flow in a liquid bridge of low-Pr fluid (Pr=0.01, As=2.0 and Ma=35.0). DNS showed a 1-T type oscillations in the liquid bridge. POD analysis revealed that the three dimensional oscillating disturbances can be decomposed into many modes. However, in this case, the temperature and velocity disturbances are well represented by two major eigen functions. Here we showed three dimensional structures of these eigen functions and their time-dependent amplitudes.

5. REFFERENCES

[1] S. Yasushiro, N. Imaishi, H. C. Kuhlmann, S. Yoda, "Numerical simulation of three dimensional oscillatory thermocapillary flow in a half zone of Pr=1 fluid", Adv. Space Res. 24, 1385-1390, 1999

[2] N. Imaishi, S. Yasushiro, T. Sato, S. Yoda, "Three dimensional numerical simulation of oscillatory Marangoni flow in a half zone of low Pr fluids", Material Research in low gravity II, Vol 3792, 344-352 (1999)

[3] N. Imaishi, S. Yasuhiro, and S. Yoda, " Numerical simulation of three dimensional oscillatory in half-zone liquid bridge of low Pr fluids" in "NASDA Technical Memorandum, Marangoni Convection Modeling Research Annual Report of FY 1999", pp.159-178 (2000)

[4] N. Imaishi, S. Yasushiro, T. Sato, S. Yoda, "Numerical simulation of three dimensional oscillatory flow in half zone bridges of low Pr fluid", Proceedings of the 4th JSME-KSME Thermal Engineering Conference, 272-282 (2000)

[5] S. Yasushiro, T. Sato, N. Imaishi, S.Yoda, "Three dimensional Marangoni flow in liquid bridge of low Pr fluid", Space Forum, 6, 39-47 (2000)

[6] N. Imaishi, S. Yasuhiro, and S. Yoda, " Numerical simulation of three dimensional oscillatory in half-zone liquid bridge of low Pr fluids" in "NASDA Technical Memorandum, Marangoni Convection Modeling Research Annual Report of FY 2000", 135-144 (2001)

[7] N. Imaishi, S. Yasuhiro, Y. Akiyama, S. Yoda, "Numerical simulation of oscillatory Marangoni flow in half-zone liquid bridge of low Prandtl number" J. Crystal Growth, 230, 164-171 (2001)

[8] N. Imaishi, S. Yasuhiro, and S. Yoda, " Numerical simulation of three dimensional oscillatory in half-zone liquid bridge of low Pr fluids" in "NASDA Technical Memorandum, Marangoni Convection Modeling Research Annual Report of FY 2001", 131-155 (2002)

[9] N. Imaishi, S. Yasuhiro, S. Yoda, "Critical condition for incipience of oscillatory flow in half-zone liquid bridge of molten tin bridge", presented at 5th China-Japan Workshop on Microgravity Science and Applications, (Dunghan, Sept.5-7, 2002)

[10] M. Lappa, S. Yasuhiro, N. Imaishi , "3D numerical simulation of on-ground Marangoni flow instabilities in liquid bridges of low Prandtl number fluid", Int. J. Num. Heat Fluid Flow, 13 (3), 309-340 (2003)

[11] S. Yasuhiro, N. Imaishi, Y. Akiyama, S. Fujino, S. Yoda, "Oscillatory Marangoni flow in half-zone liquid bridge of molten tin supported between two iron rods", submitted to J. Crystal Growth.

[12] R. Rupp, G. Mueller, G. Neumann, "Three dimensional time dependent modeling of the Marangoni convection in zone melting configurations for GaAs", *Journal of Crystal growth*, 97, (1989), 34-41

[13] M. Levenstam, G. Amberg, "Hydrodynamical instabilities of thermocapillary flow in a half-zone", J. *Fluid Mechanics*, 297, (1995), 357 -372

[14] J. Leypoldt, H.C. Kuhlmann, H.J. Rath, "Three-dimensional numerical simulation fo thermocapillary flows in cylindrical liquid bridges", J. Fluid Mech, 414, 285, (2000)

[15] Levenstam, Marten; Amberg, Gustav; Winkler, Christian, " ", Physics of Fluids, 13(4), 807-816 (2001)

[16] S. Nakamura, K. Kakimoto, T. Hibiya, "Convection visualization and temperature fluctuation measurement in a molten silicon column", Materials and fluids under low gravity (Springer), Proc. of the IXth European Symp. on Gravity-Dependent Phenomena in Physical Sciences (Berlin, Germany, 2-5 May) 1995

[17] J. H Han, Z. W. Sun, L. R. Dai, J. C. Xie, W. R. Hu, "Experiment on the thermocapillary

convection of a mercury liquid bridge in a floating half zone", J. Cryst. Growth, **169**(1), 129-135 (1996)

[18] M. Levenstam, G. Amberg, T. Carlberg, M. Andersson, "Experimental and numerical studies of thermocapillary convection in a floating zone like configuration", J. Cryst. Growth, **158**(3), 24-30 (1996),

[19] S. Nakamura, T. Hibiya, K. Kakimoto, N. Imaishi, S. Nishizawa, A. Hirata, K. Mukai, S. Yoda, T. S. Morita, "Temperature fluctuations of the Marangoni flow in a liquid bridge of molten silicon under microgravity on board the TR-I4 rocket", *Journal of Crystal Growth* ,**186**, 85, (1998).

[20] T. Hibiya, S. Nakamura, K. Mukai, Z.G. Niu, N. Imaishi, S. Nishizawa, S. Yoda, M. Koyama, "Interfacial phenomena of molten silicon: Marangoni flow and surface tension", Philos. Trans. R. Soc. London, Ser. A **356**(1739), 899-909 (1998),

[21] T. Hibiya, S. Nakamura, N. Imaishi, K. Mukai, K. Onuma, P. Dold, A. Croll, K-W Benz, S-i Yoda, "Marangoni flow of Si melt: microgravity experiments and perspective", J. Jpn. Soc. Microgravity Appl. Supplement, (1998).

[22] T. Hibiya, S. Nakamura, "Fluid flow in silicon melt with free surface", Advances in Space Research, **24**(10), 1225-1230 (1999)

[23] M. Cheng, S. Kou, "Detecting temperature oscillation in a silicon liquid bridge", J. Crystal Growth, **218** (1), 132-135 (2000)

[24] M. Sumiji, S. Nakamura, K. Onuma, T. Hibiya, "Optical measurement of resonant oscillation and marangoni convection-induced oscillation in a molten silicon surface". Jpn. J. of Applied Physics, Part 1, **39**(6A), 3688-3693 (2000),

[25] T. Azami, S. Nakamura, T. Hibiya, S. Nakamura, "The effect of oxygen on the temperature fluctuation of Marangoni convection in a molten silicon bridge" , *Journal of Crystal Growth,* **223**, pp.116-124, (2001).

[26] M. Sumiji, S. Nakamura, T. Azami, T. Hibiya, " Optical observeation of solid-melt interface fluctuation due to Marangoni flow in a silicon liquid bridge", *Journal of Crystal Growth,* **223**, pp. 503-511, (2001).

[27] T. Azami, S. Nakamura, T. Hibiya, " Observation of periodic thermocapillary flow in a molten silicon bridge by using non-contact temperature mesurements", *Journal of Crystal Growth*, **231**, 82-88 (2001).

[28] Y. K. Yang, S. Kou, "Temperature oscillation in a tin liquid bridge and critical Marangoni number dependency on Prandtl number", J. Crystal Growth, **222** (1-2): 135-143 (2001)

[29] M. Sumiji, S. Nakamura, T. Hibiya," Two-directional observation of solid-melt interface fluctuation induced Marangoni flow in a silicon liquid bridge", *Journal of Crystal Growth,* **235**, pp. 55-59 (2002).

[30] T. Azami, S. Nakamura, T. Hibiya, "Marangoni convection of molten silicon: Microgravity Experiments and Crystal Growth", *J. Jpn. Soc. Microgravity Appl.* (in Japanese), **18**, 16-25 (2001)

[31] T. Hibiya, S. Nakamura, T. Azami, M. Sumiji, N. Imaishi, K. Mukai, K. Onuma, S. Yoda, "Marangoni flow of molten silicon", Acta Astronautica, **48**(2-3), 71-78 (2001),

[32] K. Takagi, M. Ohtaka, H. Natsui, T. Arai, S. Yoda, Z. Yuan, K. Mukai, S. Yasuhiro, N. Imaishi, " Experimental study on transition to oscillatory thermocapillary flow in a low Prandtl number liquid bridge", *Journal of Crystal Growth,* **233**, pp. 399-407, (2001).

[33] K. Takagi, M. Ohtaka, H. Natsui, T. Arai, S. Yoda, "Experimental study on transition to oscillatory thermocapillary flow in molten tin column", *J. Jpn. Soc. Microgravity Appl.* (in Japanese), **18**, 11-15 (2001)

[34] S. Matsumoto, M. Ohtaka, H. Matsui, T. Arai, S. Yoda "Experimental study of thermo-capillary flow in the half-zone liquid bridge of low Prandtl number fluid", Marangoni

Convection Modeling Research, Annual Report FY 2001, 159-181 (2002)
[35] T. Suzuki, and H. Kawamura, *J. Mech. Eng. Japan (in Japanese)*, **60**-578(B), 58 (1994)
[36] H. Ozoe and K. Toh, "Dopant concentration profile in a Czochralski flow of liquid metal in a vertical or a horizontal magnetic ", *J. Crystal Growth*, **130**, 645-656 (1993).
[37] H. Natsui, S. Matsumoto, Private communication
[38] J.L. Lumley, "The structure of inhomogeneous turbulent flows," Atmospheric Turbulence and Radio Wave Propagation, A.M. Yaglom and V.I. Tatarski eds., pp. 166-178, Moskow, Nauka (1967).
[39] G. Berkooz, P. Holmes and J.L. Lumley, "The proper orthogonal decomposition in the analysis of turbulent flows," Annu. Rev. Fluid Mech.25, 539 (1993).
[40] L. Sirovich, "Turbulence and the dynamics of coherent structures Part I, II, III," Quarterly of Applied Mathematics XLV, 561 (1987).
[41] H.M. Park and D.H. Cho, "Low dimensional modeling of flow reactors," Int. J. Heat Mass Transfer **39**, 3311 (1996).
[42] H. Gunes, A. Liakopoulos and R.A. Sahan, "Low-dimensional description of oscillatory thermal convection: The small Prandtl number limit," Theoret. Comput. Fluid Dynamics, **9**, 1 (1997).
[43] R.A. Sahan, A. Liakopoulos and H. Gunes, "Reduced dynamical models of nonisothermal transitional grooved-channel flow," Phys. Fluids, **9**, 551 (1997).
[44] H. Gunes, "Low-order dynamical models of thermal convection in high-aspect ratio enclosures", Fluid Dynamic Research **30**, 1 (2002).
[45] C.J. Jing, D. Henry, H.B. Hadid, N. Imaishi, "Low-order dynamic model for low-Pr fluid flow in a laterally heated cavity", Physics of Fluid, in press (2003)

Table 1 Thermophysical properties and geometric parameters.

		Molten tin	Iron rod
Pr		0.009	-
density	ρ [kg/m3]	6793	7700
Thermal conductivity	λ [W/mK]	35.44	20.0
Specific heat	Cp [J/kgK]	242	460
Viscosity	μ [kg/ms]	$1.318 \cdot 10^{-3}$	-
Temperature coefficient of surface tension	σ_T [N/mK]	$-1.3 \cdot 10^{-4}$	-
Radius	a [m]	$1.5 \cdot 10^{-3}$	
Length of the liquid bridge [m]	L	$3.0 \cdot 10^{-3}$	
Length of the supporting rod L_r[m]		$9.0 \cdot 10^{-3}$	
Offset of the thermocouple	δ[m]	$0.5 \cdot 10^{-3}$	

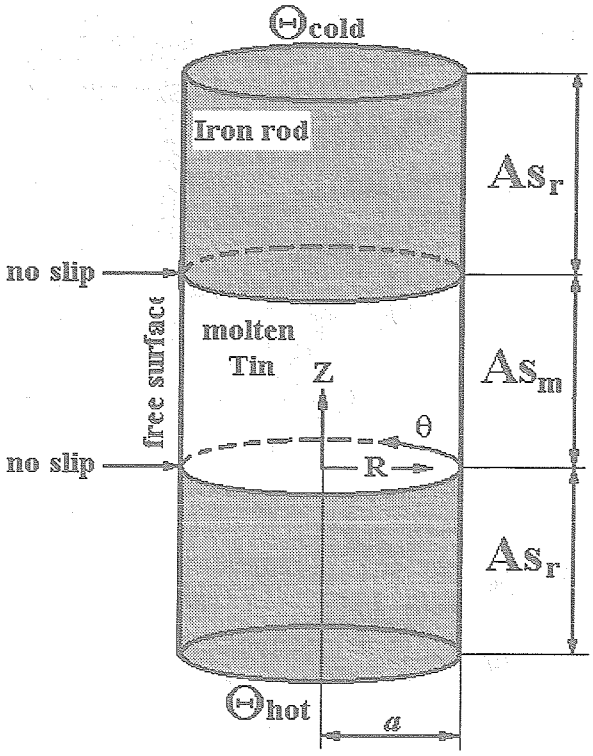

Fig.1 Schematics of a liquid bridge with two supporting rods.

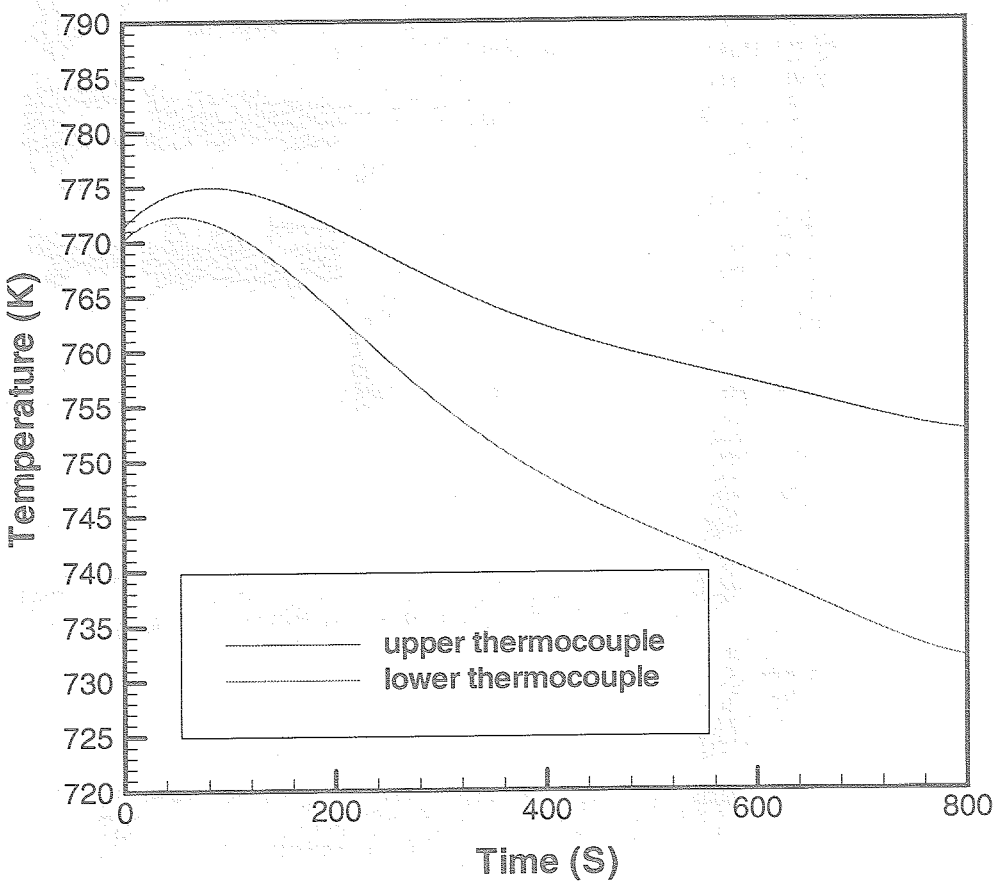

Fig.2 Time history of the temperatures imposed on the both ends of the supporting rods. Converted, by Eqs.(21) and (22), from the time records of the thermocouple EMF's.

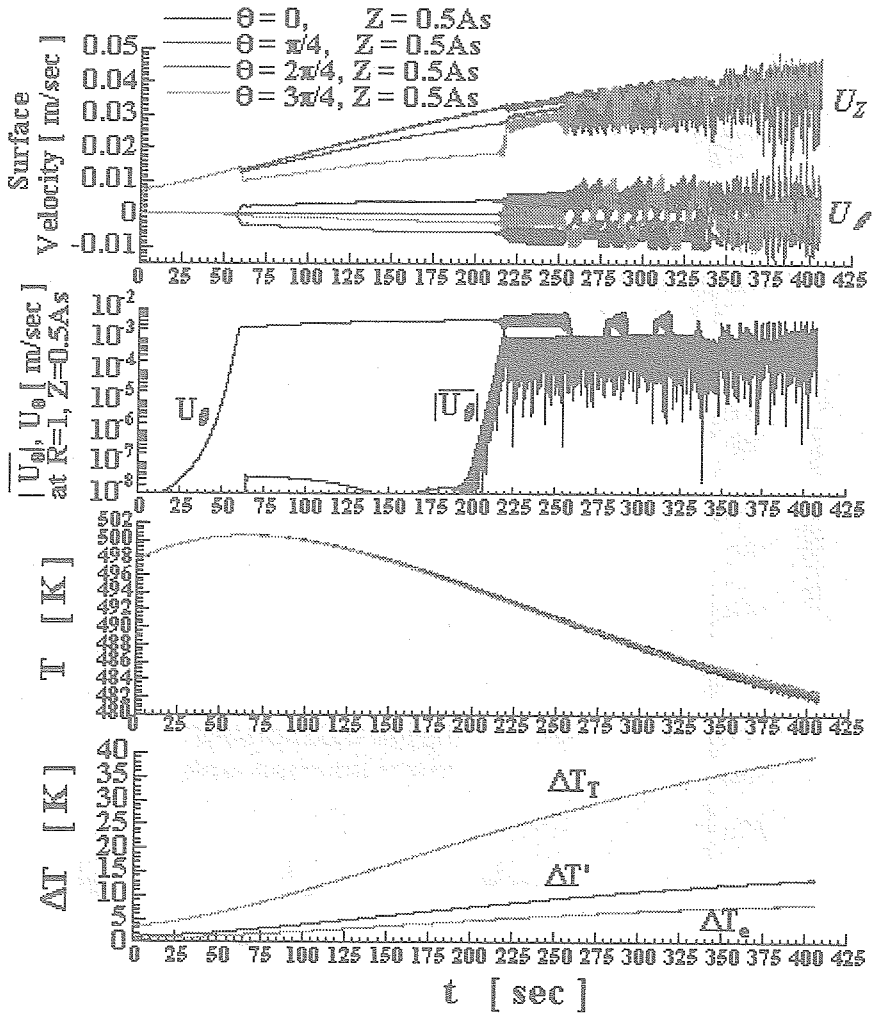

Fig.3-a Time evolutions of local velocities, averaged azimuthal velocity, local surface temperature and ΔT's (imposed over-all temperature difference between the top and bottom: $\Delta T'_T$. temperature difference between two thermocouple positions: ΔT'' and the effective temperature difference.:$\Delta T'_e$).

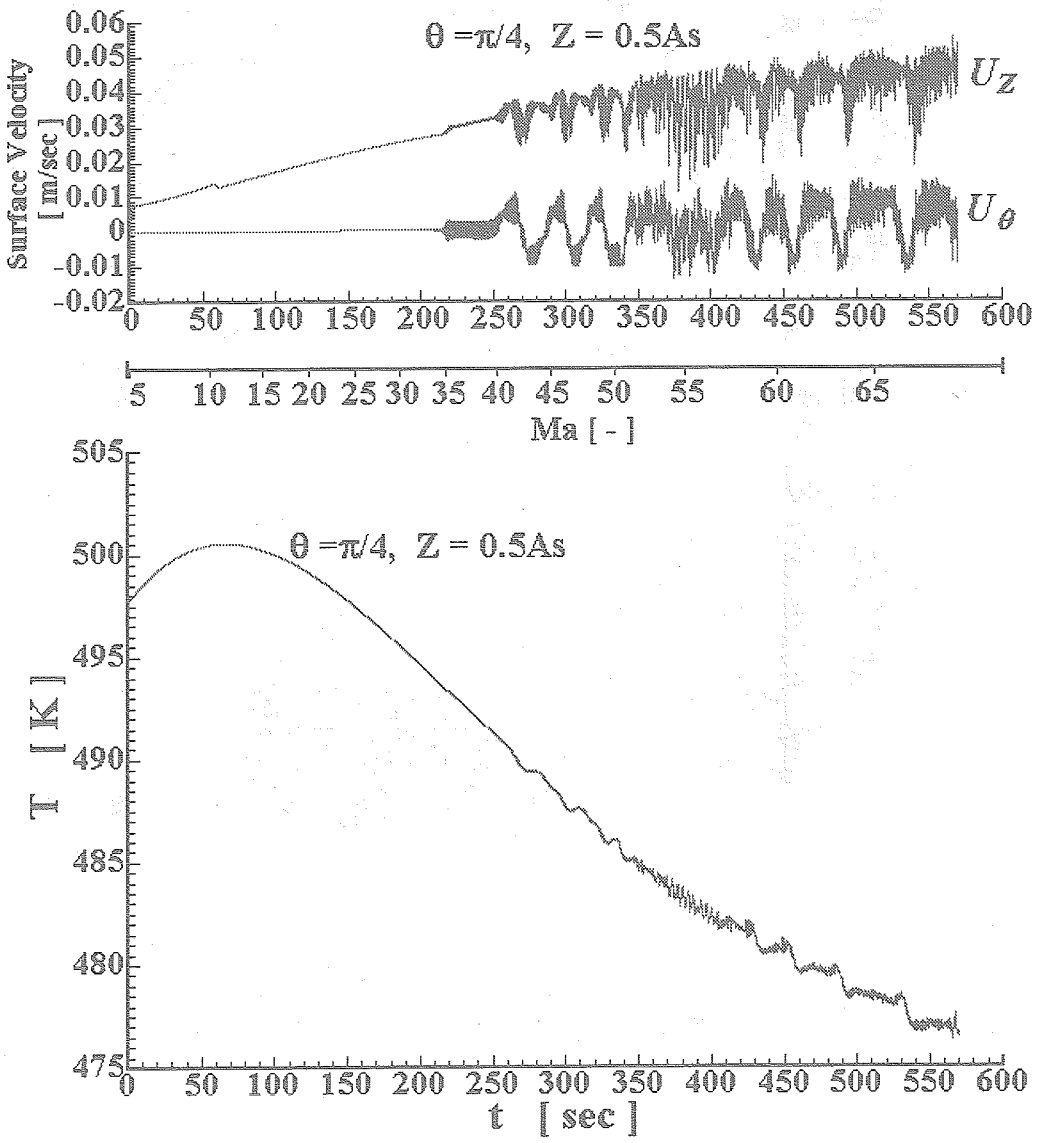

Fig.3-b Enlarged plot of a local velocities and temperature on the melt surface throughout the simulation run.

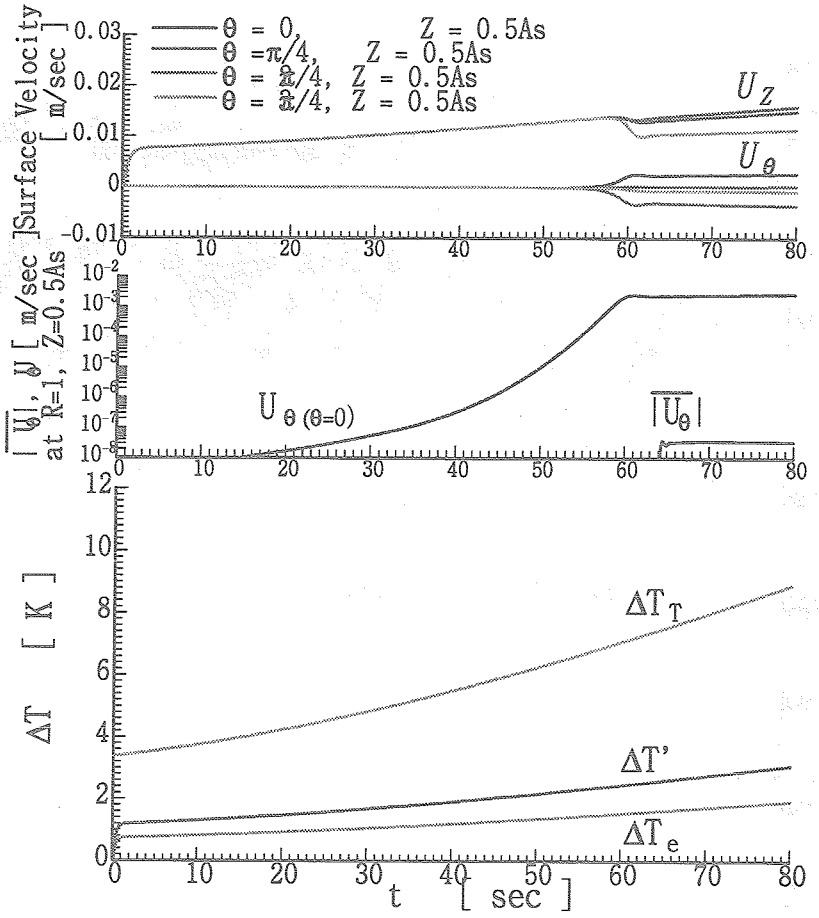

Fig.4 Results in an early stage of simulation run, showing the development of the axisimmetric Marangoni flow and the growth process of the 3-D non-oscillating flow.

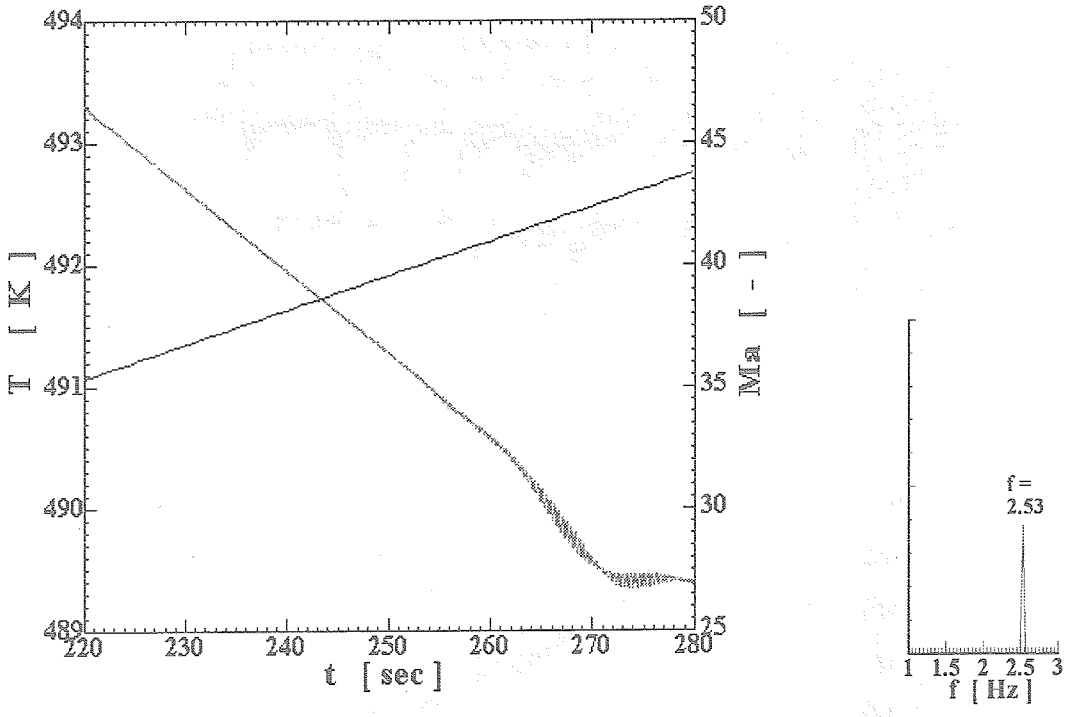

Fig.5 Enlarged plot of surface temperature at (R=1.0, θ=π/4, Z=0.5) and its FFT spectra between t=260 and 275sec..

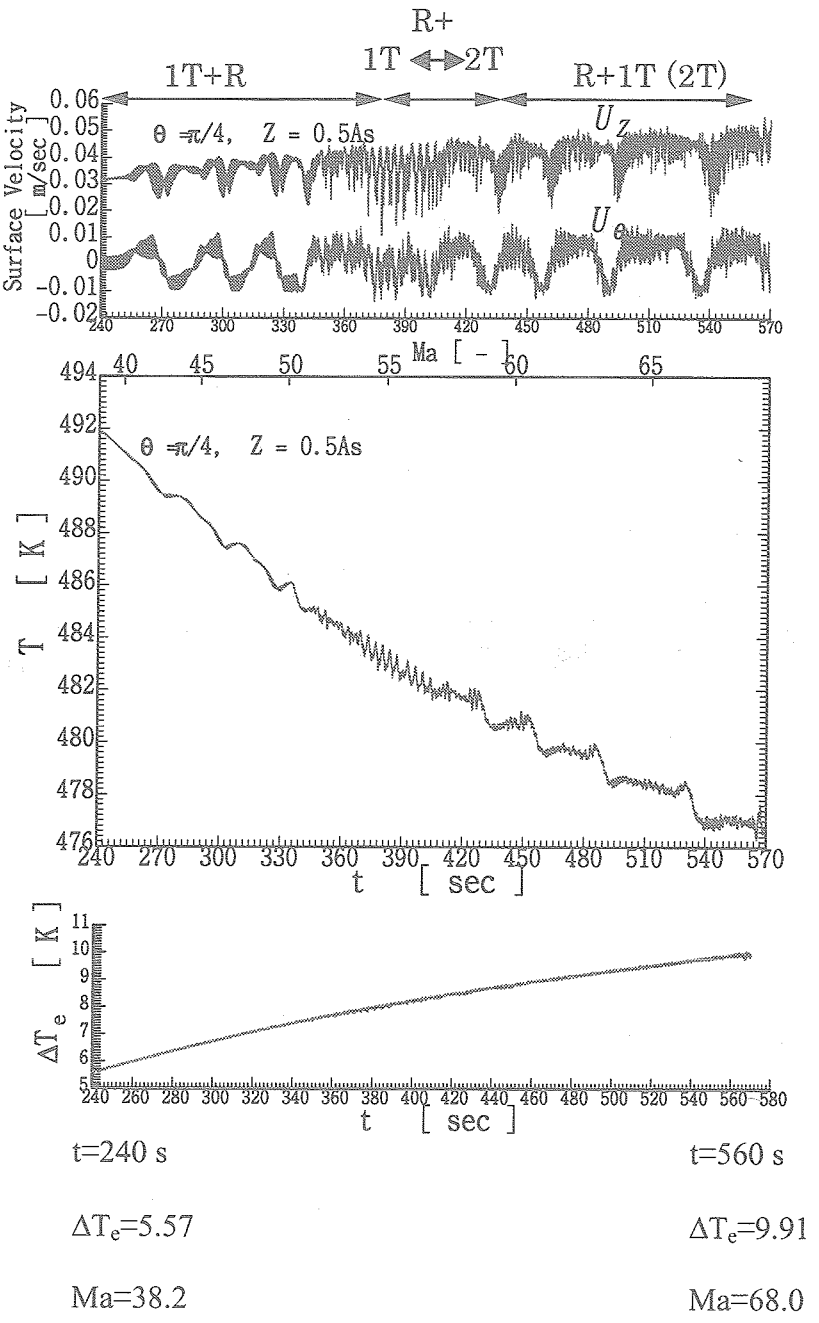

Fig.6-a Enlarged plots of local velocities, temperature on the surface (R=1.0, θ=π/4, Z=0.5) and the time records of the temperature differences. .

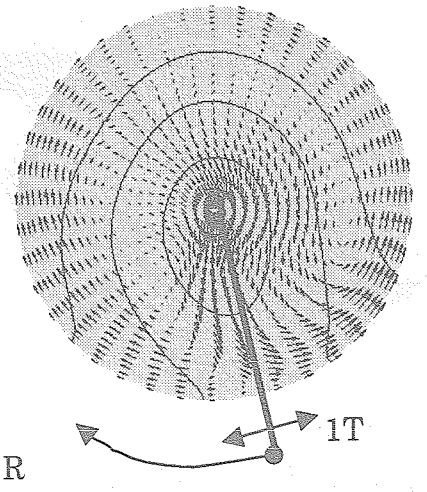

Fig.6-b Snapshots of oscillating flow field and isotherms on a horizontal cut plane at Z=0.5 during 1T+R type mode..

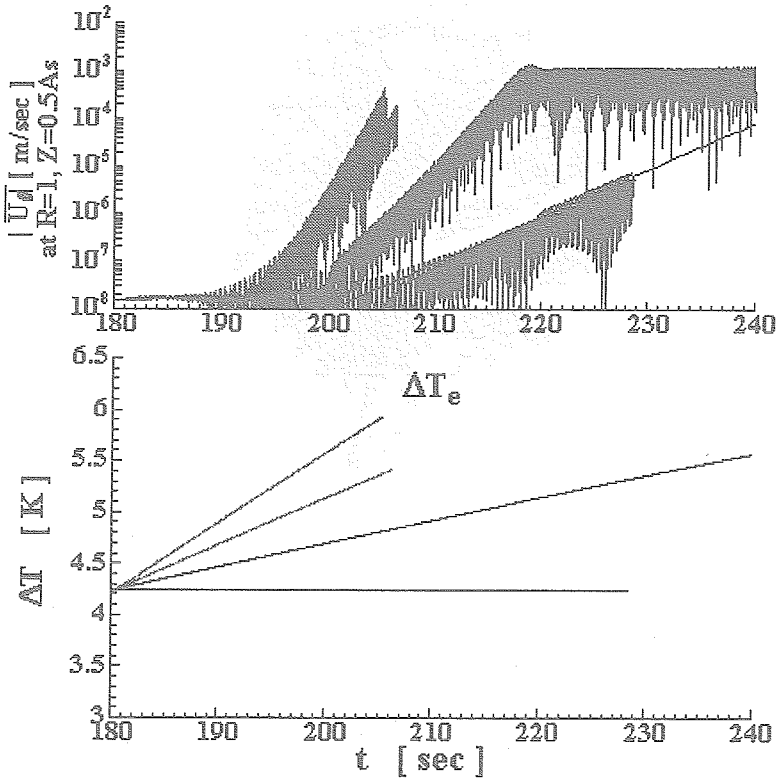

Fig.7 Effect of temperature ramp rate on the incipience of the 3-D oscillatory flow.

Flow Chart of Proper Orthogonal Decomposition (POD)

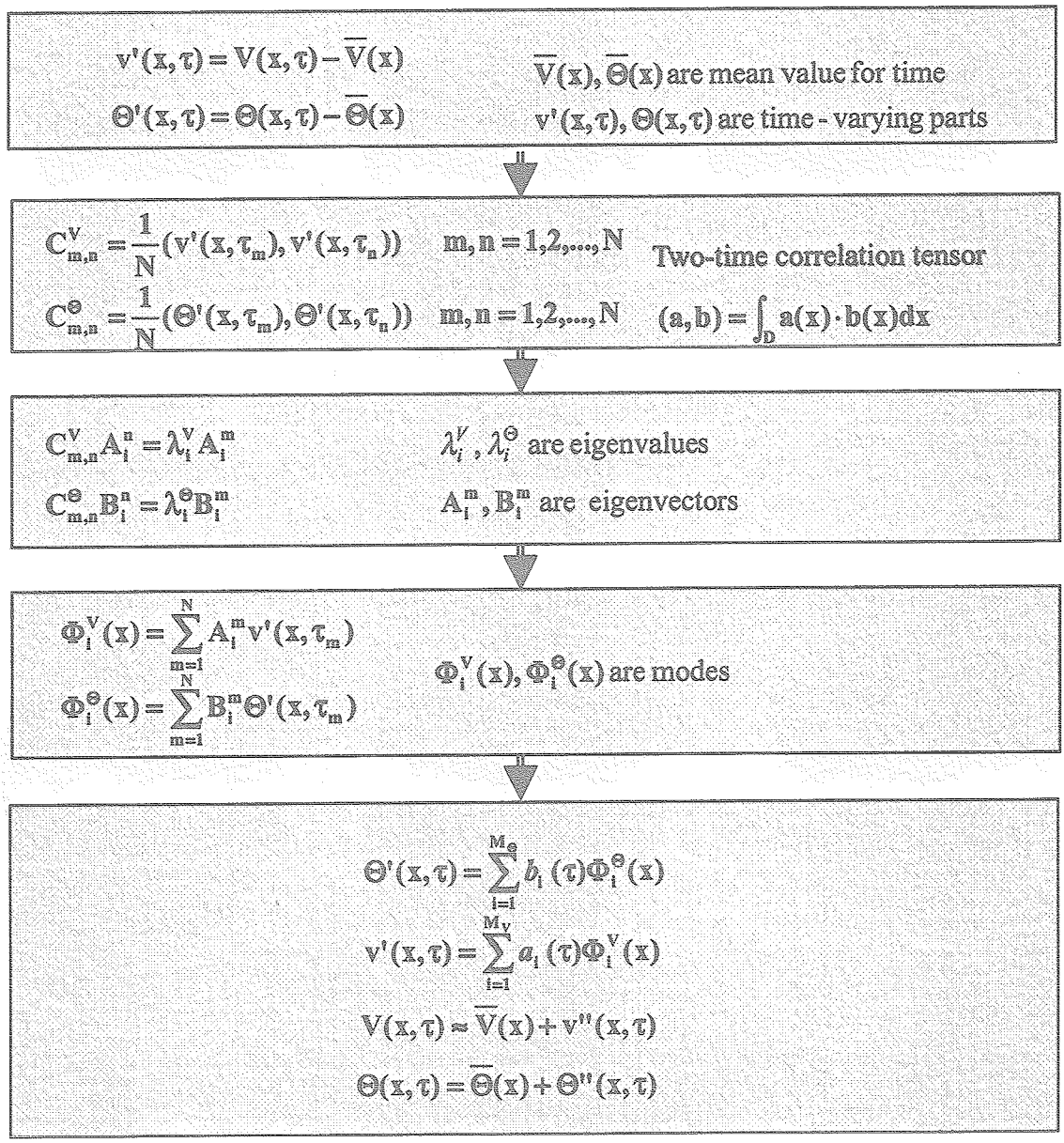

Fig.8 Flow chart of the POD.

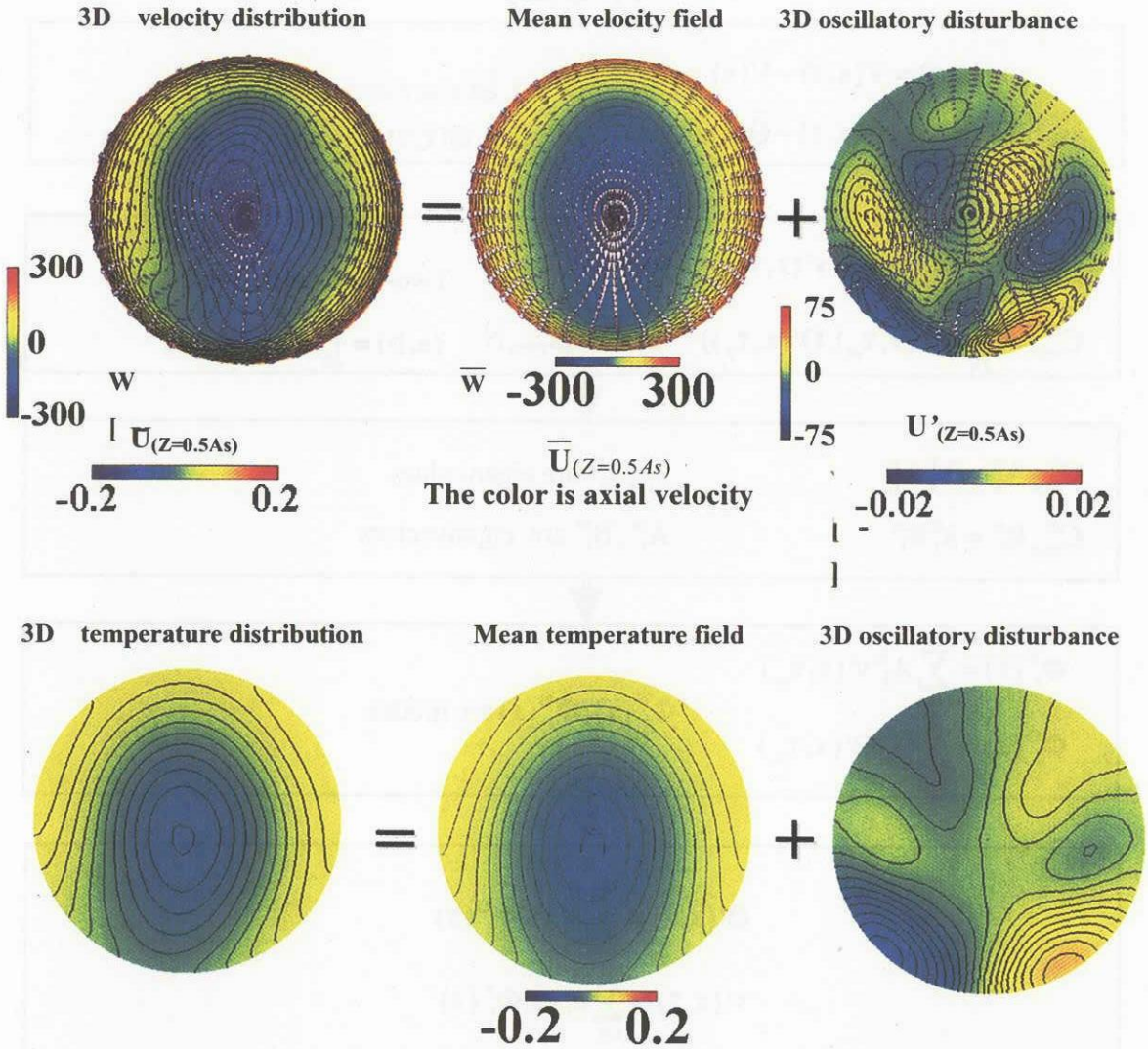

Fig.9 Time average and extraction of time-varying part of velocity and temperature.

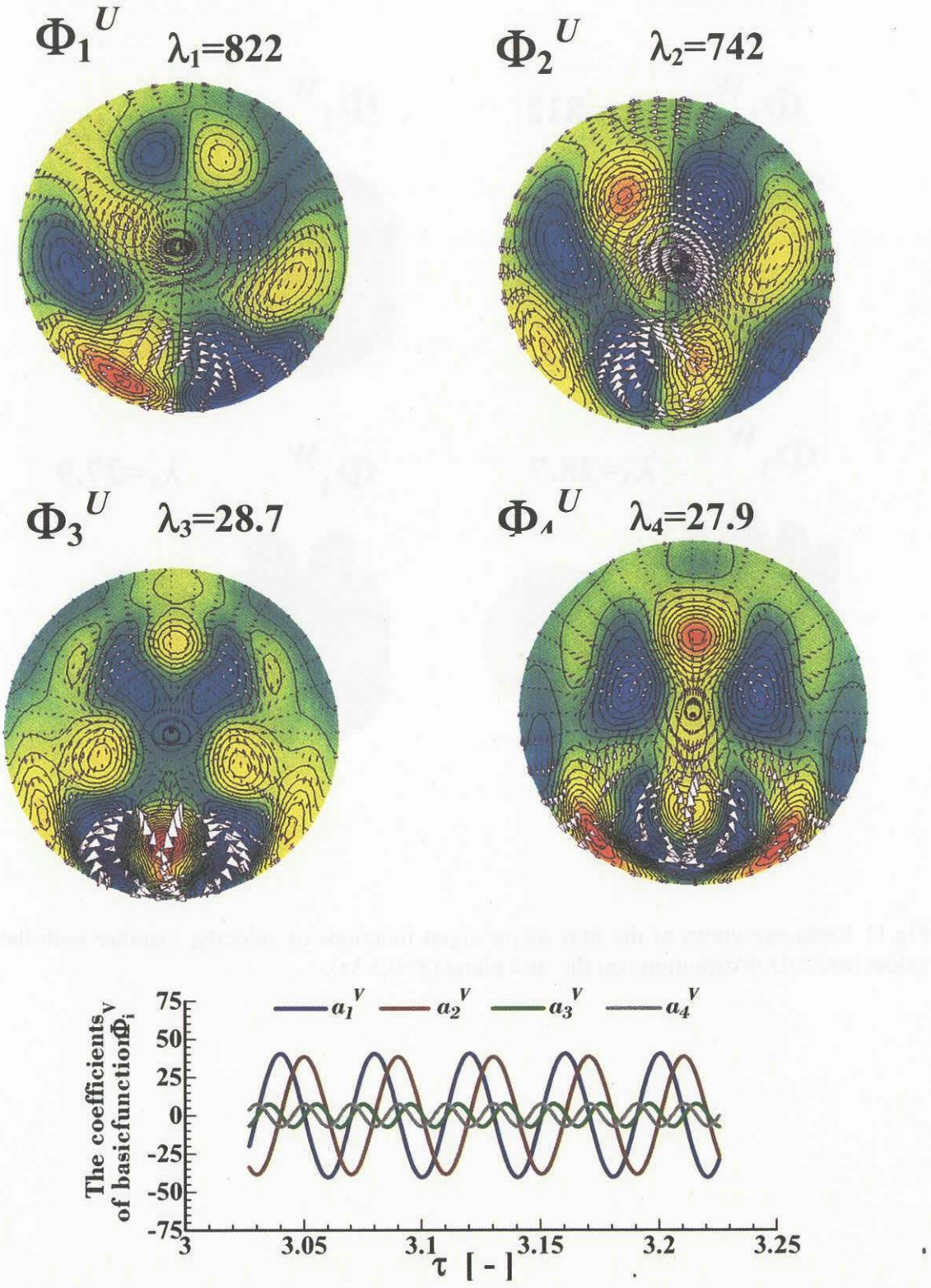

Fig.10 Four major eigen functions of velocituy, eigen values and their amplitudes as a function of time. Distribution of eigen functions on a horizontal cut at Z=0.5 color indicate W component.

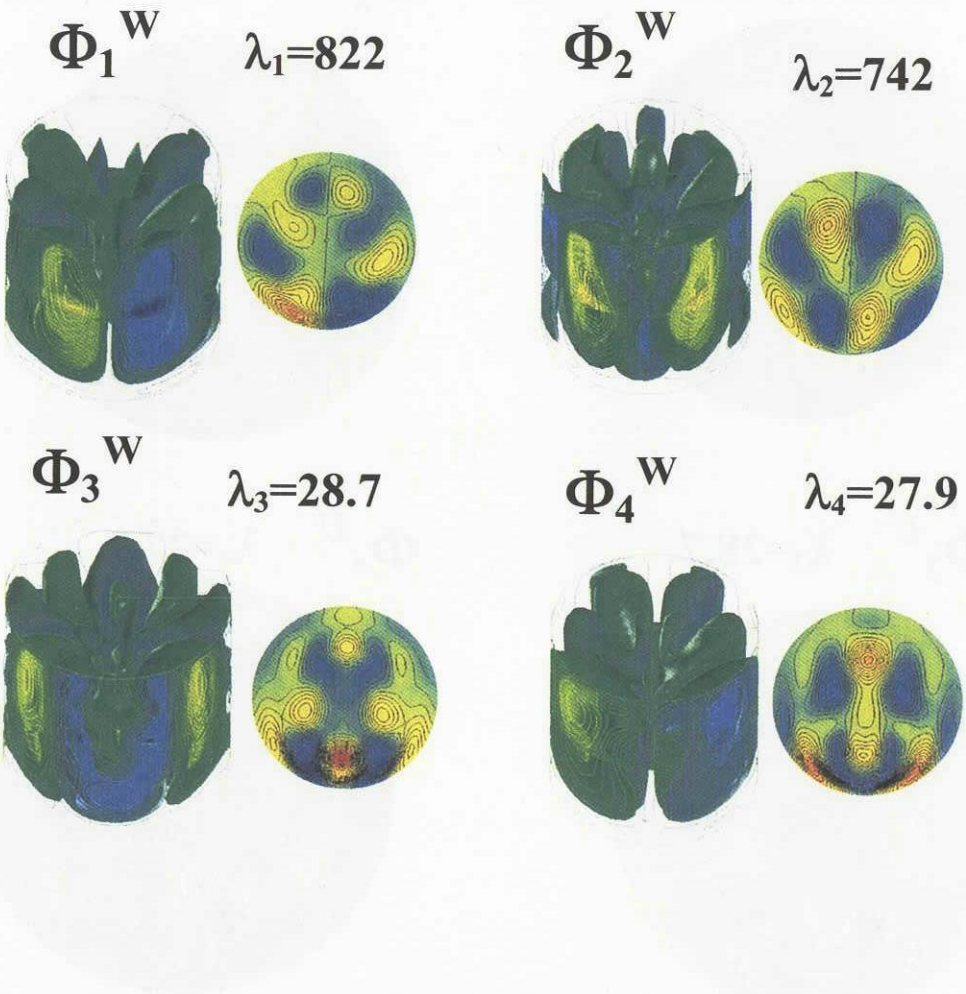

Fig.11 Birds eye views of the four major eigen functions of velocity, together with the eigen values and 2-D distributions on the mid plane (Z=0.5As).

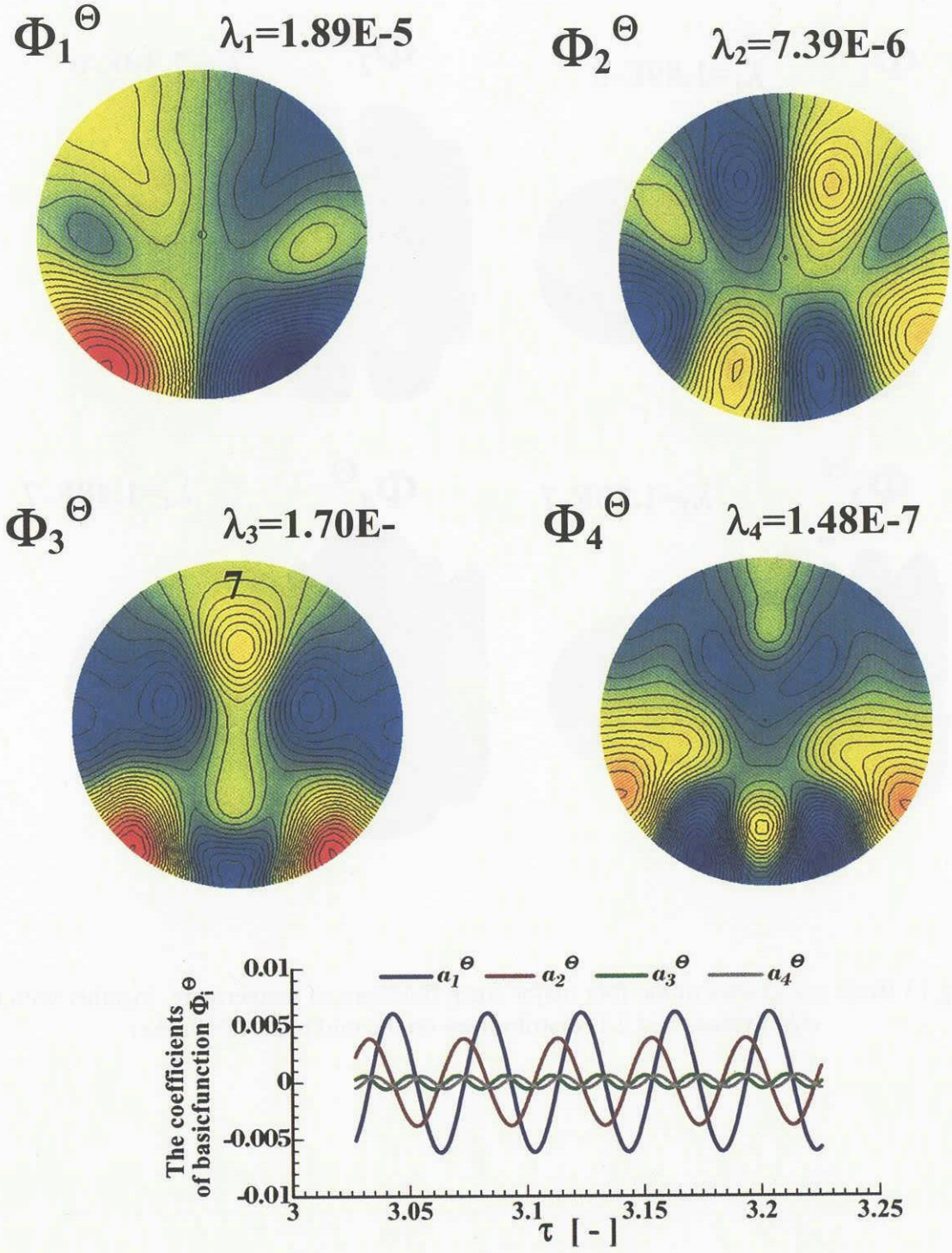

Fig.12 Four major eigen functions of temperature, eigen values and their amplitudes as a function of time. Distribution of eigen functions on a horizontal cut at Z=0.5.

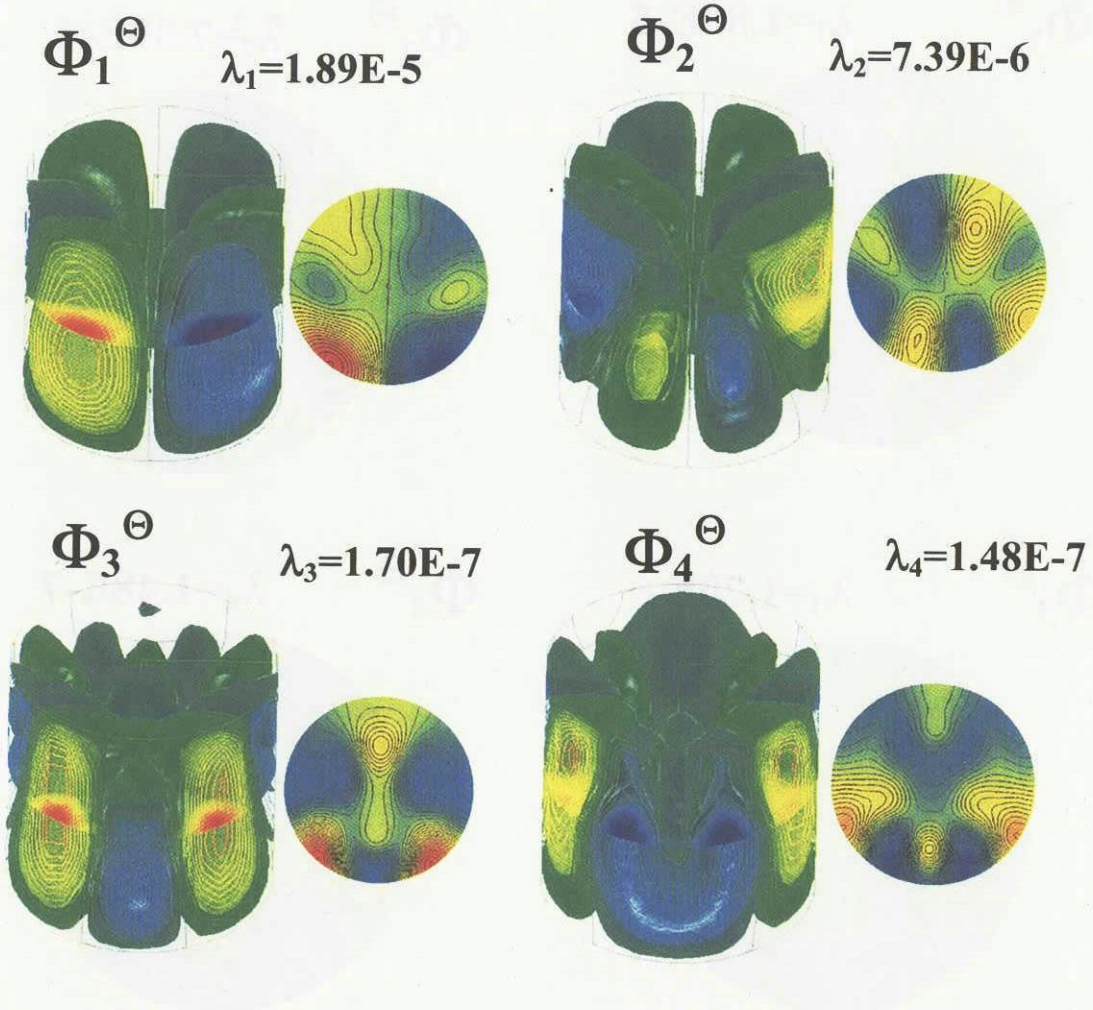

Fig.13 Birds eye gviews of the four major eigen functions of temperature, together with the eigen values and 2-D distributions on the mid plane (Z=0.5As).

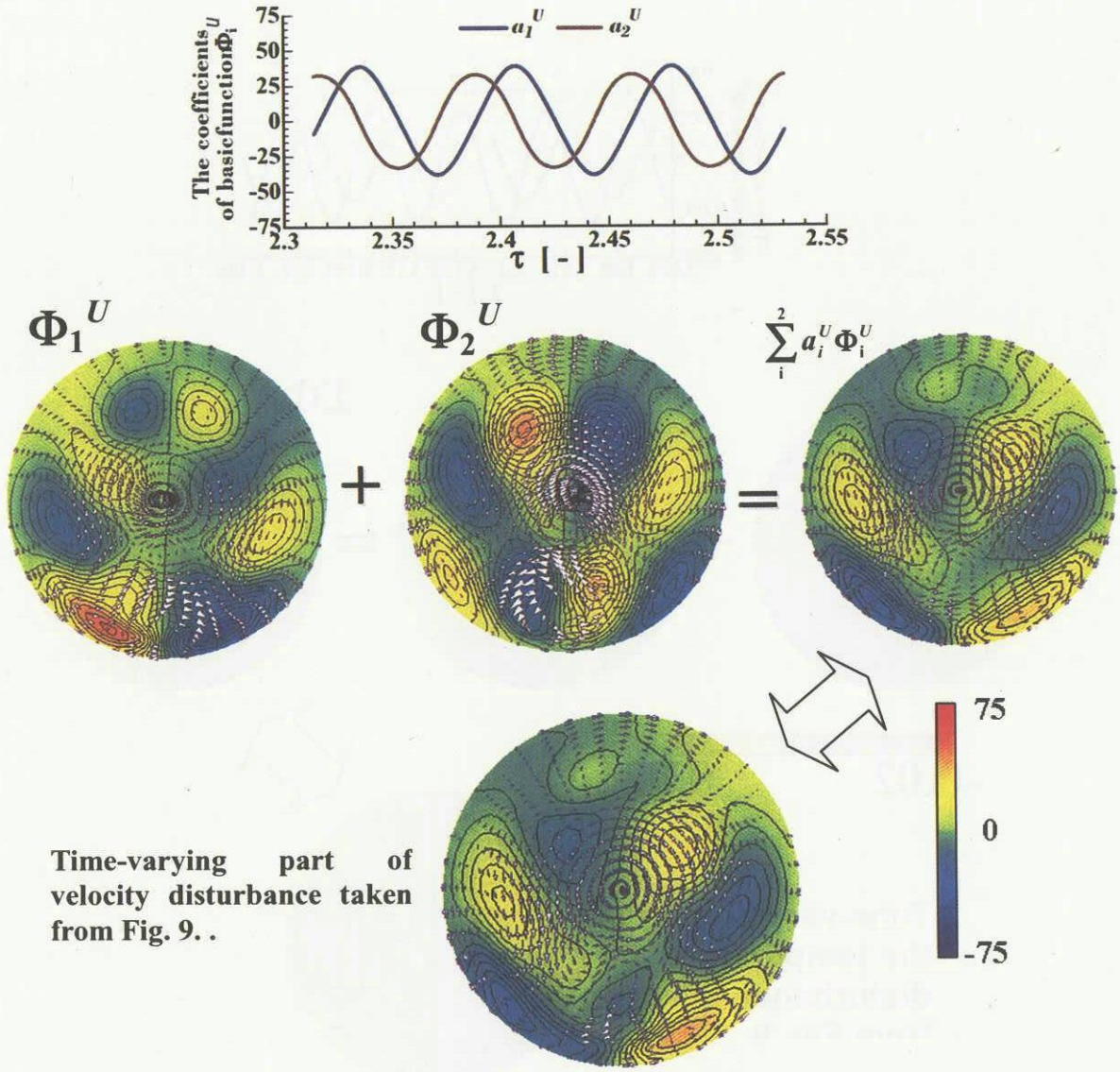

Fig.14 Synthesis of the time varying part of the velocity disturbance by sum of the two major eigen functions and their amplitudes.

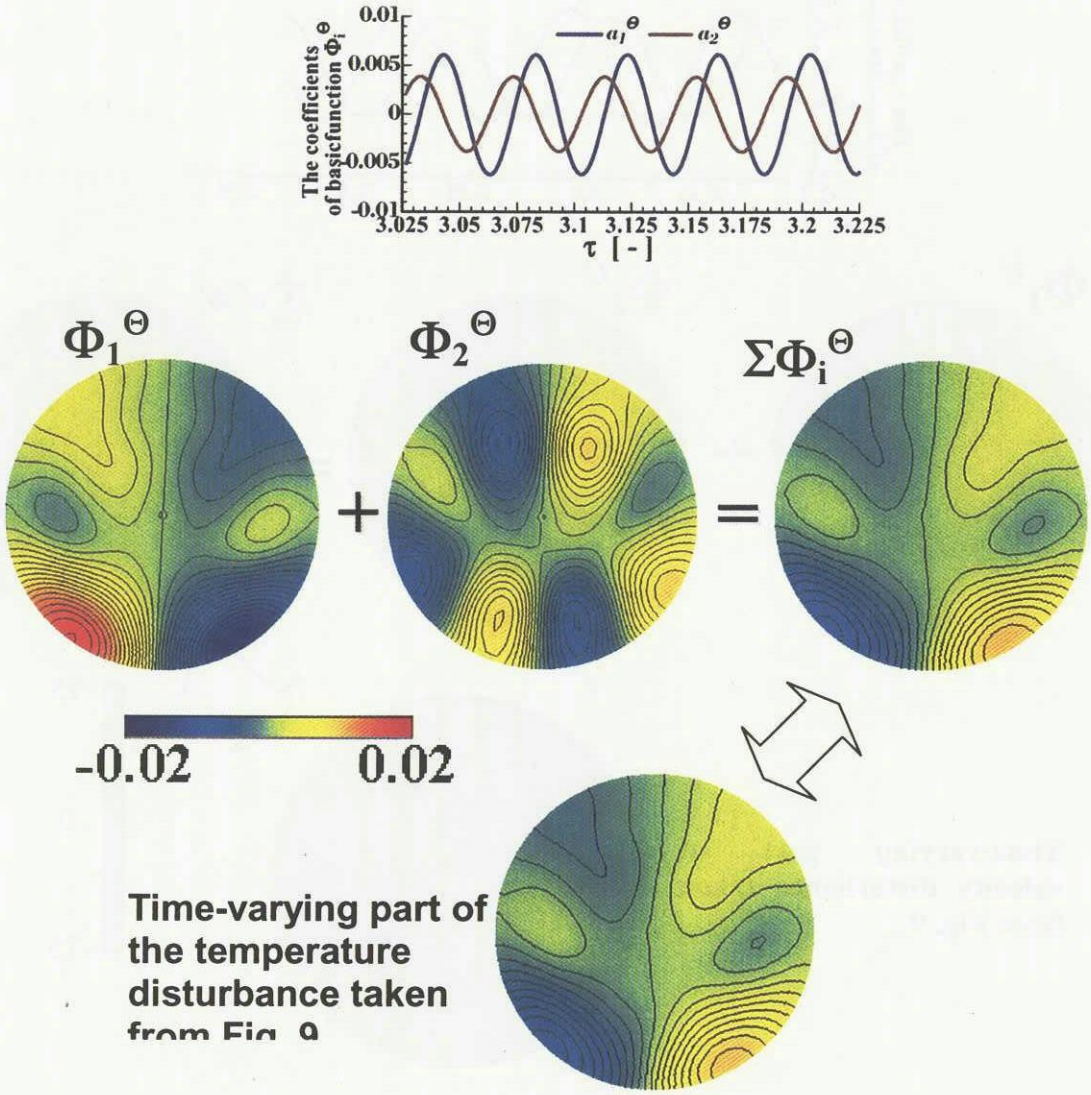

Fig.15 Synthesis of the time varing part of the temperature disturbance by sum of the two major eigen functions and their amplitudes.

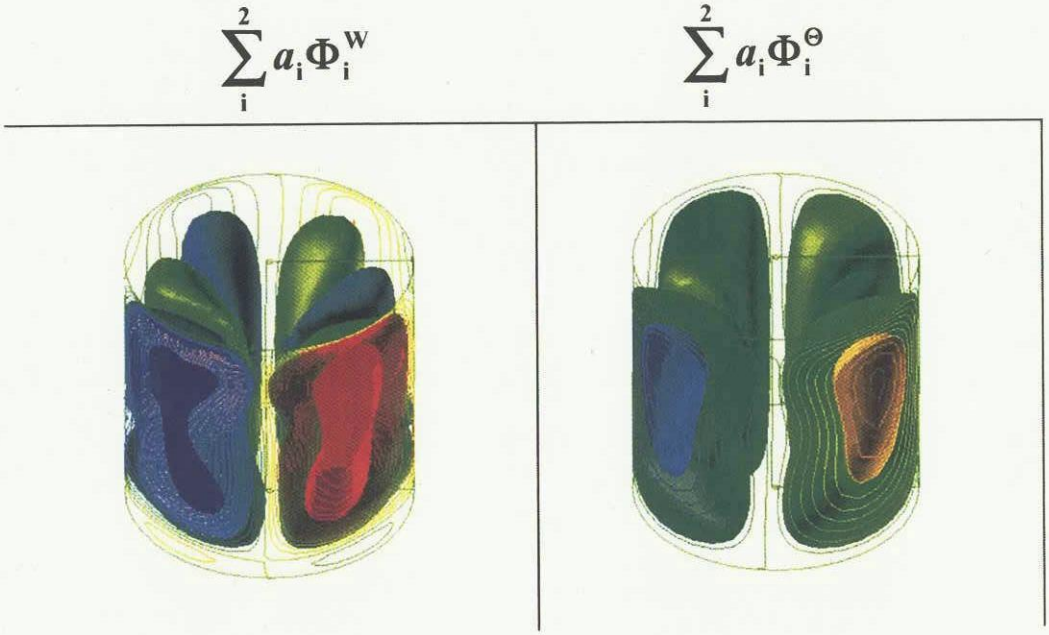

Fig.16 Bird's eye views of instantaneous spatial distributions. $\sum_{i}^{2} a_i \Phi_i^{W}$ and . $\sum_{i}^{2} a_i \ddot{O}_i^{\dot{E}}$.